Nuclear Instruments and Methods in Physics Research B 272 (2012) 100–103

Contents lists available at ScienceDirect

Nuclear Instruments and Methods in Physics Research B

journal homepage: www.elsevier.com/locate/nimb

Structural and magnetic properties of low-energy Gd implanted ZnO single crystals

P.P. Murmu [a,b,c], J. Kennedy [a,c,*], B.J. Ruck [b,c], A. Markwitz [a,c], G.V.M. Williams [c,d], S. Rubanov [e]

[a] National Isotope Centre, GNS Science, P.O. Box 31312, Lower Hutt, New Zealand
[b] School of Chemical and Physical Sciences, Victoria University of Wellington, P.O. Box 600, Wellington, New Zealand
[c] The MacDiarmid Institute for Advanced Materials and Nanotechnology, New Zealand
[d] Industrial Research Limited, P.O. Box 31310, Lower Hutt, New Zealand
[e] University of Melbourne, Inst Bio21, Melbourne, Vic. 3010, Australia

ARTICLE INFO

Article history:
Available online 2 February 2011

Keywords:
Ion implantation
Rutherford backscattering and channeling
Raman spectroscopy
Gadolinium
ZnO single crystals

ABSTRACT

We report the structural and magnetic properties of ZnO single crystals implanted with Gd ions at 40 keV. Ion beam analysis shows that after implantation up to 12% of the near-surface atoms are Gd, with most of the Gd ions occupying substitutional lattice sites. The carrier concentration of implanted films is up to several orders of magnitude larger than in unimplanted ZnO. Room temperature ferromagnetism was observed in Gd implanted and annealed ZnO. Zero-field cooled magnetisation curves reveal the presence of super-paramagnetic clusters. The annealing can cause the diffusion and/or migration of implanted ions and intrinsic defects and possibly the formation of super-paramagnetic clusters suggesting that the annealing plays a significant role towards the observed magnetic properties.

1. Introduction

Electron spin provides an additional degree of freedom that can potentially be exploited in novel semiconductor devices [1]. The combination of electron charge and spin, termed as "spintronics", can be realized in several materials such as dilute magnetic semiconductors (DMSs), rare-earth nitrides [1–3], etc. The carrier mediated mechanism was proposed to explain the observed phenomenon in DMSs [2]. Zinc oxide (ZnO) doped with transition metal (TM) atoms, up to several atomic%, has been predicted to demonstrate room temperature ferromagnetic ordering [4]. This was followed by several experimental investigations where Curie temperatures of as high as 790 K were reported [5]. However, the observation of room temperature ferromagnetism in the systems with poor conductivity or highly resistive materials suggests that there could also be some other mechanism [5]. The most likely reason could be the inclusion of magnetic ions as secondary phases and/or metallic clusters [6]. Several non magnetic ions (e.g. C) were doped into ZnO to overrule the segregation and precipitation of magnetic ions into the material [7]. The room temperature ferromagnetism has also been observed in pure ZnO, which suggests that the intrinsic defects can also play a significant role towards the observed property [8]. Oxygen vacancies (V_o) and zinc interstitials (Zn_i) are common intrinsic defects present in the ZnO which can occur during sample growth and post growth treatments. Thus, room temperature ferromagnetism is highly sensitive to the preparation technique and post growth treatments along with the impurity magnetic ions. Recently, high magnetic moment has been observed in GaN [9] and ZnO doped with rare earth (RE) elements [10,11]. RE elements usually have higher magnetic moment compared to TM elements. RE dope ZnO has mainly been investigated in terms of optical properties [12,13]. Recent reports on gadolinium (Gd) doped ZnO suggest that the coupling between Gd ions is ferromagnetic which can be enhanced by electron doping [14]. The aim of this paper is to investigate the structural properties of Gd implanted into ZnO single crystals and subsequent effects on the magnetic property.

2. Experimental procedure

The Zn-face of hydrothermally grown ZnO(0 0 0 1) was implanted with 40 keV Gd ions using a low energy ion implanter [15–17]. Implanted Gd fluences range from 6.7×10^{14} to 3.0×10^{16} cm^{-2} resulting in 0.7 to 12 at.% Gd in the near surface region of ZnO, with average implantation depth of 12 nm and maximum depth of 25 nm as was found by theoretical calculation using DYNAMIC-TRIM [18] (see Fig. 1). The implanted samples were subsequently annealed in a vacuum chamber with base pressure $P_b \sim 1 \times 10^{-7}$ mbar [17]. Rutherford backscattering spectrometry (RBS) measurements were performed for compositional analysis and depth profiling with a collimated 2 MeV He^+ beam. Rutherford backscattering spectrometry and channeling (RBS/C) analyses were carried out to estimate the crystalline quality upon implantation and annealing. Structural modifications were investigated applying

* Corresponding author at: National Isotope Centre, GNS Science, 30 Gracefield Road, Lower Hutt, New Zealand. Tel.: +64 4 570 4771; fax: +64 4 5704657.
E-mail address: j.kennedy@gns.cri.nz (J. Kennedy).

0168-583X/$ - see front matter © 2011 Elsevier B.V. All rights reserved.
doi:10.1016/j.nimb.2011.01.041

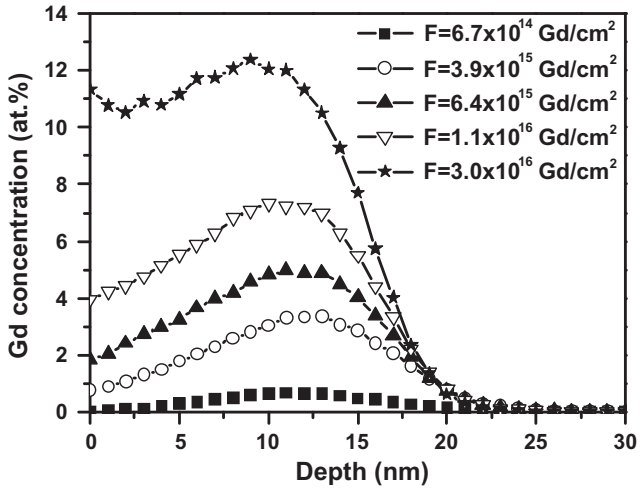

Fig. 1. Gd depth profiles calculated with DYNAMIC-TRIM for Gd implanted at 40 keV into ZnO in the fluence range from 6.7×10^{14} to 3.0×10^{16} cm^{-2}.

Raman spectroscopy using a Jobin–Yvon LabRam micro-Raman system at ambient temperature. An Ar^+ laser with wavelength 514 nm was an excitation source and the spectra were collected in backscattering geometry with a liquid nitrogen-cooled charge coupled device detector. Hall effect measurements were performed at room temperature using the Van der Pauw geometry. A Quantum Design MPMS superconducting quantum interference device (SQUID) was employed to study the magnetic properties of the films.

3. Results and discussion

To characterise the depth profile and lattice location of the implanted Gd ions RBS and RBS/C measurements were carried out on all samples. The retained doses, composition and the thickness information were extracted using the Rutherford Universal Manipulation Program (RUMP) [15]. Fig. 2 shows the RBS spectra of an unimplanted and a sample implanted with 3.9×10^{15} Gd cm^{-2} and vacuum annealed at 650 °C in random and channeled conditions. The RBS spectra demonstrate the near-surface nature of the implantation, consistent with the results shown in Fig. 1. The channeled spectrum is considerably attenuated, indicating that this sample retains relatively good crystallinity after implantation.

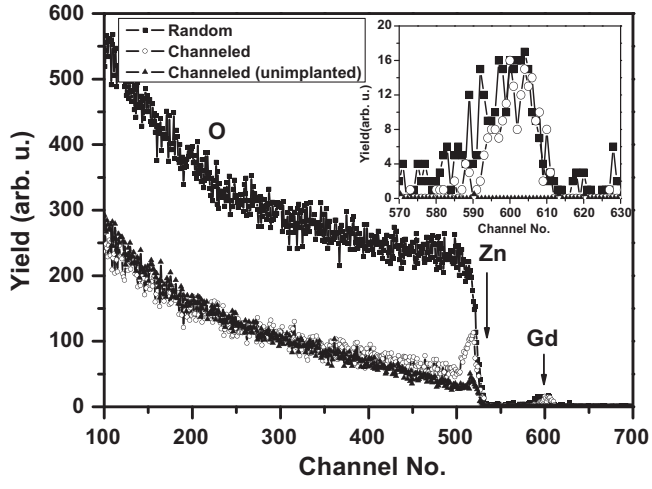

Fig. 2. Random and ⟨0 0 0 1⟩-aligned RBS spectra of an unimplanted, 3.9×10^{15} Gd cm^{-2} implanted and vacuum annealed at 650 °C ZnO. The inset shows an expanded view of the Gd peak.

In Fig. 3(a) and (b) the RBS/C measurements carried out along the <0 0 0 1> direction of the ZnO lattice are shown for the sample implanted with 3.9×10^{15} Gd cm^{-2}, both before and after annealing at 650 °C. The ratio of the RBS yield in channeling and random, termed as X_{min}, was collected as a function of the incident beam angle for both Zn and Gd. The $^{Zn}X_{min}$ value of around 27% for the unannealed sample is somewhat larger than the value of 7% for unimplanted ZnO, suggesting that the material is partly crystalline and well below the amorphization threshold. After annealing $^{Zn}X_{min}$ reduces to 22%. The corresponding values of $^{Gd}X_{min}$ are 56% and 64% for as implanted and annealed samples, respectively. The data for Zn and Gd follow similar trends, suggesting that both ions are subjected to similar types of lattice disorder, although the larger $^{Gd}X_{min}$ values imply that the Gd ions are more disordered overall. The fraction of Gd ions located on Zn substitutional sites can be estimated from [12,13].

$$Gd_{Zn} = \frac{(1 - {}^{Gd}\chi_{min})}{(1 - {}^{Zn}\chi_{min})}$$

Applying this formula around 60% of the Gd ions in the unannealed sample occupy substitutional lattice sites. After annealing the estimated Gd ions at the substitutional sites reduced to 47%, possibly suggesting the occurrence of some clustering in the annealed samples, consistent with the observations reported by Alves et al. for Er implanted ZnO [12] and Wahl et al. [13]. The latter suggest an annealing temperature of around 1050 °C is required for complete recovery of the crystalline damage [13]. However, annealing at such elevated temperatures is likely to enhance clustering and potentially lead to the out-diffusion of the implanted ions.

Further investigation of the effects of implantation and subsequent annealing of the ZnO:Gd films was carried out by Raman spectroscopy. The characteristic Raman modes in ZnO are $A_1 + 2B_1 + E_1 + 2E_2$ [19]. The non-polar E_2 modes have two wavenumbers E_2^{high} and E_2^{low} associated with the motion of the O and Zn sub-lattices, respectively. The modes A_1 and E_1 are polar modes, and can be split into transverse (TO) and longitudinal optical (LO) phonons. The E_2, A_1 (TO), and E_1 (TO) modes are observed when the incident radiation is perpendicular to the *c*-axis of the sample, whereas E_2 and A_1 (LO) modes are observed when the incident radiation is parallel to the *c*-axis [20]. Fig. 4(a) shows the Raman spectra obtained from the samples implanted with fluences between 6.7×10^{14} and 3.0×10^{16} Gd cm^{-2}. The spectra are dominated by the strong O and Zn related peaks observed at 438 cm^{-1} (E_2^{high}) and 100 cm^{-1} (E_2^{low}), which are characteristic of high-quality ZnO. The peak near 331 cm^{-1} arises due to the second-order phonon, $2E_2(M)$, scattering [19]. However, there is a broad feature from 520 cm^{-1} to 600 cm^{-1} which consists of two peaks at 540 cm^{-1} and 575 cm^{-1}. The peak at 575 cm^{-1} can be attributed to the A_1 (LO) mode of ZnO, a mode that is usually observed due to disorder in ZnO [20,21]. Observation of this peak has been attributed to the presence of structural defects such as oxygen vacancies (V_o) and zinc interstitials (Zn_i) or their complexes [22]. The peak at 540 cm^{-1} is from two phonon scattering from the LA phonon branch, which is also disorder-induced. Fig. 4(b) displays the Raman spectra collected for unimplanted, 3.9×10^{15} Gd cm^{-2} as-implanted and 3.9×10^{15} Gd cm^{-2} vacuum annealed samples. As expected annealing helps to recover the implantation induced disorder, similar to the observations of Schumm et al. for air annealed ZnO:Mn [21]. The fact that this is possible after vacuum annealing, which might induce some oxygen loss, implies that the observation of the 540 cm^{-1} and 575 cm^{-1} peaks is not closely related to the

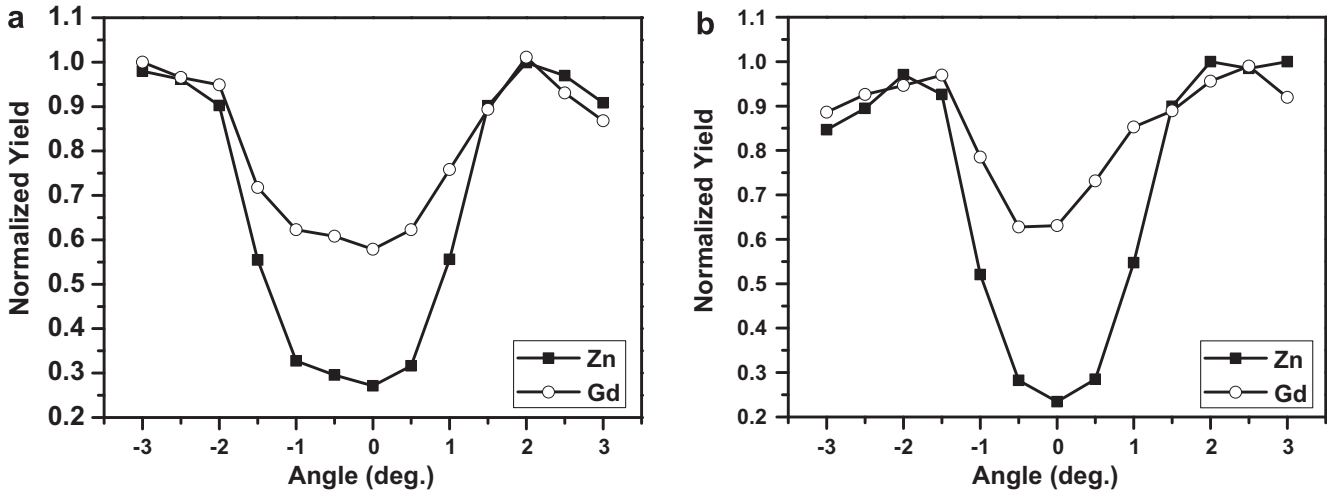

Fig. 3. (a) Angular scan around ⟨0 0 0 1⟩ for a sample implanted with 3.9×10^{15} Gd cm^{-2}. (b) Angular scan around ⟨0 0 0 1⟩ of the same film after annealing at 650 °C.

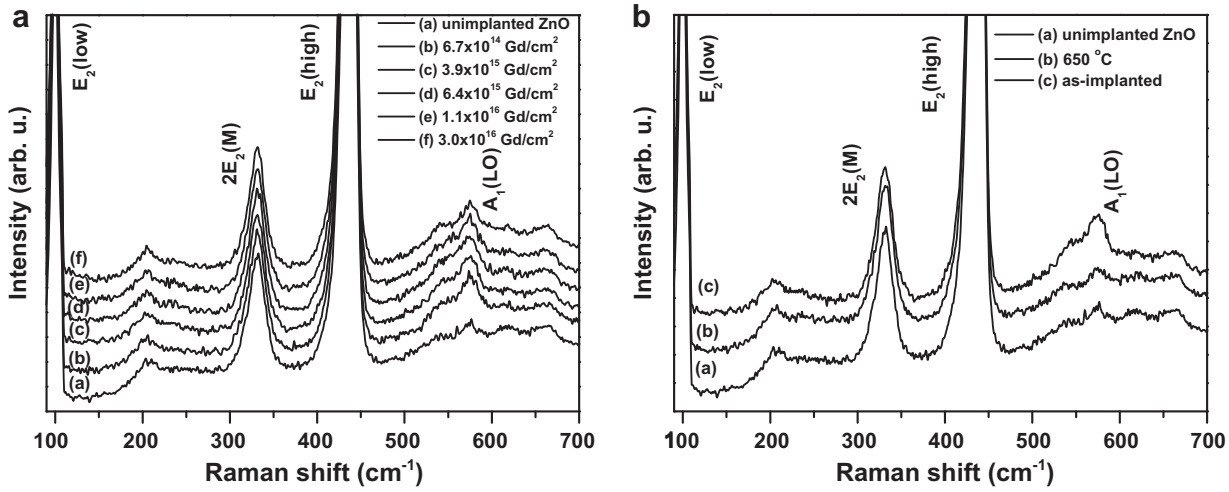

Fig. 4. (a) Raman spectra of ZnO implanted between 6.7×10^{14} and 3.0×10^{16} Gd cm^{-2}. (b) Raman spectra of unimplanted and 3.9×10^{15} Gd cm^{-2} implanted and 650 °C annealed ZnO.

presence of oxygen vacancies, and must therefore be due to some other defects.

Hall effect measurements performed in the Van der Pauw geometry at room temperature showed that electrons are the major charge carriers. The unimplanted ZnO has a carrier concentration of $\sim 8 \times 10^{13}$ cm^{-3}, as quoted by the supplier. The implantation of 3.9×10^{15} Gd cm^{-2} led to an increase of the carrier concentration up to 1.8×10^{20} cm^{-3}, assuming the conduction takes place in the top 40 nm of the sample. Annealing caused a slight further enhancement of the surface layer carrier concentration to 2.7×10^{20} cm^{-3}, possibly due to the enhancement of intrinsic defects such as V_o [10].

The magnetisation reversal measurements were carried out at 5 K and 300 K for unimplanted and 6.7×10^{14} to 6.4×10^{15} Gd cm^{-2} implanted and annealed ZnO, sweeping the field from −1 T to 1 T. Unimplanted ZnO exhibited diamagnetism even at 5 K. The typical hysteresis loops are shown in Fig. 5(a) for 3.9×10^{15} Gd cm^{-2} implanted and 650 °C annealed ZnO. The inset depicts the saturation magnetic moment for 6.7×10^{14}–6.4×10^{15} Gd cm^{-2} implanted and annealed ZnO. It ranges from 10^{-3} emu cm^{-3} at 5 K where the magnetic moment unit refers to the total sample volume. It is to be noted that the diamagnetic background contribution from the ZnO substrate has been corrected for all the samples. There was no ferromagnetic ordering in the as-implanted samples. However clear evidence for ferromagnetic order that persist to room temperature can be observed upon annealing the samples, which suggests the ferromagnetic ordering temperature is above 300 K.

To investigate the ferromagnetic ordering temperature field cooled (FC) and zero-field cooled (ZFC) measurements were performed with an applied field of 100 Oe. For ZFC, the samples were first cooled down to 5 K from room temperature at zero field and measured while increasing the temperature up to 360 K. FC measurements were performed while decreasing the temperature from 360 K to 5 K. Fig. 5(b) shows the FC/ZFC magnetisation curves for 3.9×10^{15} Gd cm^{-2} implanted and annealed ZnO. It can be seen that the critical temperature is greater than 300 K. The ZFC curve shows an initial increase of the magnetic moment up to 40 K which suggests the presence of size distributed super-paramagnetic clusters. The possible cluster formation can be caused by the diffusion and/or migration of the implanted ions during the annealing process. To understand the nature of the ferromagnetism it is important to consider possible impurities. ZnGd and Gd metal have Curie temperatures of 268 K and 293 K, respectively, whereas,

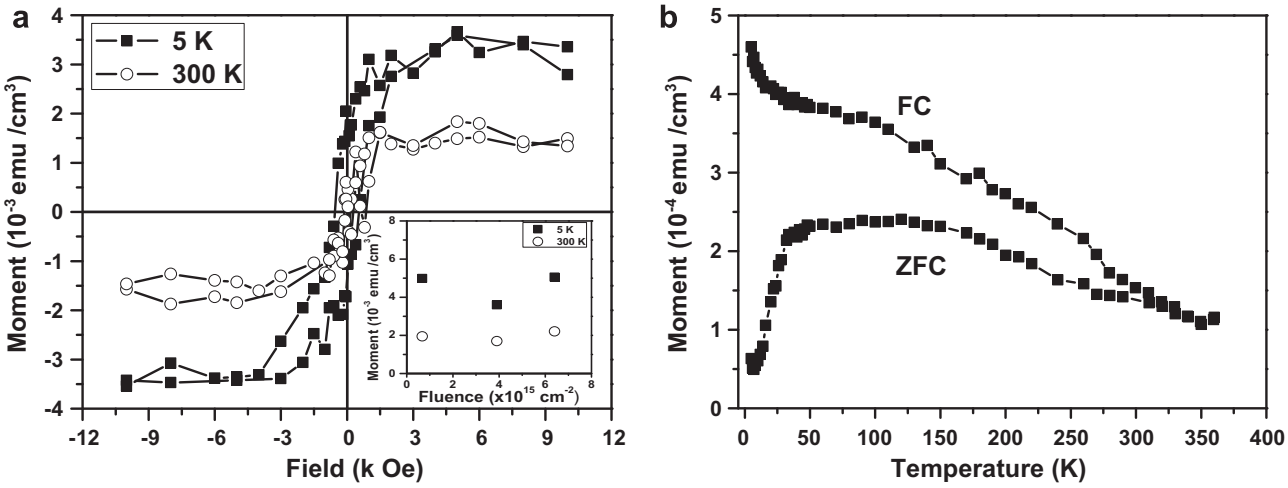

Fig. 5. (a) Magnetisation hysteresis loops of 3.9×10^{15} Gd cm^{-2} implanted and 650 °C annealed ZnO, at 5 K and 300 K. Inset shows the saturation magnetic moment at 5 K and 300 K from 6.7×10^{14} to 6.4×10^{15} Gd cm^{-2} implanted and annealed ZnO. (b) Field cooled and zero-field cooled magnetisation curves obtained using a measurement field of 100 Oe of 3.9×10^{15} Gd cm^{-2} implanted and annealed ZnO.

Gd_2O_3 is paramagnetic at room temperature [11]. Thus, these are unlikely to contribute towards the observed ferromagnetism above room temperature. The field cooled measurement also shows a paramagnetic contribution below about 40 K. A similar trend has been reported in the literature [23], Martinez et al. suggested that the non-homogenous distribution of Co atoms in Co-doped ZnO leads to a combination of ferromagnetic and paramagnetic Co ions, depending on their surroundings in the lattice. Based on the results, it seems like that a similar effect is occurring in our samples.

Dietl et al. suggested that the ferromagnetism in DMS materials should arise due to the (indirect) coupling among the magnetic ions at the substitutional lattice sites [2]. However, in our case, ferromagnetic ordering is enhanced upon annealing in the ZnO:Gd. The implantation and annealing enhance the free charge carrier concentration which can establish the indirect ferromagnetic coupling among diluted ions. Potzger et al. suggested that the optimum concentration of ions must be present in the material which can be helped by free charge carriers to mediate the ferromagnetic coupling [11]. The enhancement of ferromagnetic ordering has been observed in pure ZnO by Banerjee et al. They proposed that the annealing leads diffusion of V_o and cluster formation which interact through isolated F^+ centres or limited electrons delocalisation can lead to ferromagnetism by double exchange mechanism [8].

4. Summary

The effect of Gd implantation into the near surface region and subsequent annealing on the structural and magnetic properties of ZnO single crystals has been investigated. RBS/C showed that the Gd ions can be successfully introduced primarily into substitutional lattice sites. Annealing leads to the diffusion of ions which most likely reduces the number of Gd ions at substitutional lattice sites. The, implantation induced disorder, around 575 cm^{-1}, was found which is a common feature of ion implantation induced crystalline defects. Annealing did not make a significant difference in the carrier concentration in contrast to significant impact on the observed ferromagnetism. Further investigation is underway to address the observed ferromagnetism with the varying Gd concentration and annealing conditions.

Acknowledgement

The project has been carried out under the research contract (C05X0408) from the Foundation for Research Science and Technology of New Zealand.

References

[1] S.A. Wolf, D.D. Awschalom, R.A. Buhrman, J.M. Daughton, S. von Molnar, M.L. Roukes, A.Y. Chtchelkanova, D.M. Treger, Science 294 (2001) 1488.
[2] T. Dietl, H. Ohno, F. Matsukura, J. Cibert, D. Ferrand, Science 287 (2000) 1019.
[3] S. Granville, B.J. Ruck, F. Budde, A. Koo, D.J. Pringle, F. Kuchler, A.R.H. Preston, D.H. Housden, N. Lund, A. Bittar, G.V.M. Williams, H.J. Trodahl, Phys. Rev. B 73 (2006) 235335.
[4] K. Sato, H. Katayama-Yoshida, Semicond. Sci. Technol. 17 (2002) 367.
[5] C. Song, K.W. Geng, F. Zeng, X.B. Wang, Y.X. Shen, F. Pan, Y.N. Xie, T. Liu, H.T. Zhou, Z. Fan, Phys. Rev. B 73 (2006) 024405.
[6] J.H. Park, M.G. Kim, H.M. Jang, S. Ryu, Y.M. Kim, Appl. Phys. Lett. 84 (2004) 1338.
[7] H. Pan, J.B. Yi, L. Shen, R.Q. Wu, J.H. Yang, J.Y. Lin, Y.P. Feng, J. Ding, L.H. Van, J.H. Yin, Phys. Rev. Lett. 99 (2007) 127201.
[8] S. Banerjee, M. Mandal, N. Gayathri, M. Sardar, Appl. Phys. Lett. 91 (2007) 182501.
[9] S. Dhar, O. Brandt, M. Ramsteiner, V.F. Sapega, K.H. Ploog, Phys. Rev. Lett. 94 (2005) 037205.
[10] M. Ungureanu, H. Schmidt, H. von Wenckstern, H. Hochmuth, M. Lorenz, M. Grundmann, M. Fecioru-Morariu, G. Güntherodt, Thin Solid Films 515 (2007) 8761.
[11] K. Potzger, S. Zhou, F. Eichhorn, M. Helm, W. Skorupa, A. Mücklich, J. Fassbender, T. Herrmannsdörfer, A. Bianchi, J. Appl. Phys. 99 (2006) 063906.
[12] E. Alves, E. Rita, U. Wahl, J.G. Correia, T. Monteiro, J. Soares, C. Boemare, Nucl. Instr. Meth. Phys. Res. B 206 (2003) 1047.
[13] U. Wahl, E. Rita, J.G. Correia, E. Alves, J.P. Araújo, The ISOLDE Collaboration, Appl. Phys. Lett. 82 (2003) 1173.
[14] H. Shi, P. Zhang, S.S. Li, J.B. Xia, J. Appl. Phys. 106 (2009) 023910.
[15] J. Kennedy, A. Markwitz, B.J. Ruck, S.M. Durbin, W. Gao, J. Electron. Mater. 36 (2007) 472.
[16] J. Kennedy, D.A. Carder, A. Markwitz, R.J. Reeves, J. Appl. Phys. 107 (2010) 103518.
[17] P.P. Murmu, J. Kennedy, A. Markwitz, B.J. Ruck, AIP Conf. Proceedings 1151 (2009) 185.
[18] J.P. Biersack, Nucl. Instr. Meth. Phys. Res., Sect. B 27 (1987) 21.
[19] J.M. Calleja, M. Cardona, Phys. Rev. B 16 (1977) 3753.
[20] F. Decremps, J. Pellicer-Porres, A.M. Saitta, J.C. Chervin, A. Polian, Phys. Rev. B 65 (2002) 092101.
[21] M. Schumm, M. Koerdel, S. Müller, H. Zutz, C. Ronning, J. Stehr, D.M. Hofmann, J. Geurts, New J. Phys. 10 (2008) 043004.
[22] C.J. Young, T.S. Jeong, M.S. Han, J.H. Kim, J. Cryst. Growth 261 (2004) 526.
[23] B. Martínez, F. Sandiumenge, Ll. Balcells, J. Arbiol, F. Sibieude, C. Monty, Phys. Rev. B 72 (2005) 165202.